Experimental Observations of Two-Dimensional Blade-Vortex Interaction

Earl R. Booth Jr.*
NASA Langley Research Center, Hampton, Virginia

Blade-vortex interaction is the source mechanism for a prominent impulsive noise created by rotorcraft. An experimental study of two-dimensional blade-vortex interaction was performed to determine controlling parameters governing the strength of the blade-vortex interaction process. The interaction process is shown to involve a combination of effects on the vortex, including changes in trajectory and distortion of the vortex core shape while the blade undergoes significant transient loading. Calculations of the acoustic field produced by the interaction using measured unsteady blade surface pressure data are presented. The effects of the interaction process on the blade and the vortex are shown to be increased by both reduction of blade-to-vortex spacing and increase in blade loading.

Nomenclature

a/c = nondimensional vortex major axis length
c = blade model chord length, 20.32 cm
c_g = vortex generator chord length, 15.24 cm
$\hat{C}_l$ = blade unsteady lift coefficient
c_0 = acoustic velocity in still air, m/s
f = vortex generator oscillation frequency, Hz
k = reduced frequency, $\pi f c_g / U_\infty$
l = force per unit area on the fluid, Pa
M = Mach number
n = unit vector normal to blade panel
p = pressure, Pa
p' = acoustic pressure, Pa
r = length of radiation vector, m
$\hat{r}$ = unit vector along radiation direction
S = blade surface, m^2
t = time, s
U, U_∞ = test section total and mean velocity, respectively, m/s
u = streamwise perturbation velocity, m/s
v = velocity in y/c direction, m/s
$x/c, y/c$ = nondimensional length in streamwise direction and normal to streamwise direction, respectively
α = blade angle of attack, deg
Γ = vortex circulation, m^2/s
ω = vorticity vector, rad/s

Subscripts

L = loading term
n = normal to the panel surface
r = component in the direction of the observer
ret = retarded time
T = thickness term

Received Dec. 12, 1988; revision received March 22, 1989.

*Research Engineer.

Introduction

BLADE-VORTEX interaction (BVI) noise is a prominent impulsive noise generated by helicopters in powered descent. This noise is caused by rotor inflow conditions where the vortex wake produced by the rotor is ingested into the rotor disk and the embedded blade tip vortices come close to, or actually collide with, a rotor blade. This aeroacoustic problem is difficult to study because it is a localized, transient problem in the midst of a complex three-dimensional time-dependent flow. In order to isolate the salient details of the interaction process, study of a simpler problem is useful.

Early theoretical work by Widnall[1] suggested that the strength of BVI was a function of the angle between the vortex and the blade at the moment of interaction. The most intense interaction occurs when the axis of the vortex is parallel to the span of the blade. This case, which produces the most intense and impulsive noise, is called two-dimensional blade-vortex interaction. Nakamura[2] reached a similar conclusion but related his results to the blade acoustic planform and also pointed out the importance of the leading edge of the rotor blade in the interaction process.

Analytically, two-dimensional BVI is a simpler case to work with since one of the spatial coordinate directions is eliminated. Several researchers, among them Hardin and Lamkin,[3] and Wu et al.,[4] have examined the low-speed two-dimensional blade-vortex interaction. George and Chang,[5] and McCroskey and Goorjian[6] have examined the transonic case. Results from these analytical studies, however, have not produced a list of parameters controlling the interaction process, which could lead to a noise reduction method applicable to rotorcraft. Hardin and Lamkin[7] have produced a paper that takes a fundamental look at the parameters controlling noise production from the process, and their conclusions are supported by the experimental data presented in this paper.

Experimentally, however, two-dimensional BVI is not simple at all since a vortex must be produced normal to the flow velocity. One possible method for simulating two-dimensional BVI is to immerse an airfoil model representing a rotor blade section in the fully developed wake behind an airfoil oscillating at high reduced frequency. Early flow visualization of this type of wake was provided by Bratt,[8] who used an airfoil in plunging oscillation at small amplitude. The resulting wake was composed of alternating positive and negative vortex filaments. A similar wake can be produced by oscillating an airfoil about its quarter-chord, and such a wake has been chosen as

the incident flowfield by a number of investigators,[9,10] including the author.[11] However, in the earlier work, the author noted that the wake vortices were spaced too closely together to separate the effects of individual vortices on the stationary blade model.

In order to guide modification of the oscillating airfoil wake to increase the vortex separation, some means of calculating the resulting modified wake shape were required. A method used by Katz and Weihs[12] employed a finite vortex model to calculate wakes behind an airfoil in sinusoidal plunging oscillation. The finite vortex model, coupled with transient lift functions derived from analyses by Theodoresen[13] and Sears,[14] was used to calculate vortex wakes produced by several nonsinusoidal "tailored" oscillation pitch schedules, one of which was selected for subsequent studies. The resulting vortex wake exhibited vortex separation on the order of five blade chord lengths.[15]

The objective of this paper is to present and discuss the significant results from the two-dimensional BVI experimental program. First, flow surveys have been performed using hot-wire anemometry to determine the strength and vorticity distribution of the wake vortices produced during both the sinusoidal and tailored airfoil oscillation conditions.[16] Then, using the tailored wake as the incident vortex flowfield, subsequent work involved flow visualization using a laser light sheet triggered by the oscillating airfoil, from which vortex trajectory, size, and distortion are obtained. Unsteady blade surface pressures on the blade model have been measured and used to compute transient blade loading[17] and the acoustic field produced by the interaction. The results from these experiments provide a glimpse into the BVI process and reveal that the strength of the interaction appears to be diminished by increasing the blade-to-vortex miss distance or by decreasing the steady loading of the rotor blade.

Experimental Methods

Test Facility

The experiment was performed in the Quiet Flow Facility in NASA Langley Research Center's Aircraft Noise Reduction Laboratory. This facility is composed of two acoustic wind-tunnel circuits, one for high speed and one for low speed, terminating in an anechoic chamber. For this experiment, the low-speed leg of the facility was used as a low-turbulence, very low-speed wind tunnel. The test was run at a flow speed of 6.1 m/s measured at the exit of the flow nozzle. Details of laboratory construction and operation may be found in Ref. 18.

Description of Vortex Generator

A two-dimensional vortex was created by oscillating an airfoil model, called a vortex generator, about its quarter-chord station. The oscillation of the vortex generator, combined with the freestream velocity, created a periodic wake with very organized vortex structures on the order of five blade chord lengths apart. The vortex generator consisted of a 15.24-cm chord NACA 0012 airfoil model driven by a variable-speed electric motor through a captured cam transmission. The airfoil spanned a two-dimensional test section downstream of the flow nozzle, upstream of the blade model. Oscillation amplitude and pitch schedule were fixed by interchangeable cams. Oscillation rate was varied by motor speed. Vortex generator position was monitored with a 500-pt/revolution optical encoder with a 1-pt/revolution reset signal mounted on the drive motor shaft. Advantages of the system were that pitch schedule and oscillation amplitude were fixed, reducing test condition matching to flow speed and oscillation rate matching.

Description of Experimental Setup

The experimental apparatus used for this series of experiments consisted of a basic test stand and various specialized test setups. This section will describe the experimental setups and the type of data obtained with each arrangement.

In general, the experimental apparatus consisted of a flow nozzle connecting the 1.2-m diam flow duct to a 0.30×0.45-m rectangular nozzle. Two side plates were connected to long sides of the rectangular nozzle to form a two-dimensional test section. The vortex generator was mounted between the side plates. Large windows were located in the side plates downstream of the vortex generator, allowing visual access to the test section. An airfoil model representing a rotor blade section was suspended between the side plates in the test section by a mechanical traverse. The flow speed, measured at the exit of the rectangular nozzle, was maintained at 6.1 m/s.

Hot-Wire Measurements

The flow generated by the vortex generator using the tailored pitch schedule was surveyed to determine the strength of the vortex filament in the wake used in the two-dimensional BVI study. A cross-wire probe was transversed to several points along a survey line positioned along the x/c station, where the leading edge of the blade model is placed during the interaction study. No blade model was present in the test section during the flow survey. At each survey point, the flow velocity and direction were recorded for a period greater than one oscillation cycle. The velocity data were then used to compute vorticity data from which the circulation of the vortex could be determined. A more complete account of the flow survey is given in Ref. 16.

One of the most significant findings of the flow survey is that the mean flow velocity U_∞ is 4.6 m/s at the x/c station surveyed. Although the flow speed was maintained at 6.1 m/s at the exit of the nozzle entering the two-dimensional test section, the action of oscillating the vortex generator slows the mean flow speed by 25% by the time the flow reaches the blade model. Another significant result was that the flowfield in the test section was shown to be two-dimensional for approximately 85% of the test section span. This result indicates the degree to which the experiment produces an idealized two-dimensional flow and justifies using 1 c wide panels for the acoustic calculations described below.

Velocity time history data were reduced into u and v components, using the flow velocity and angle to compute U and v and then subtracting the measured freestream velocity from U to yield u. Using the flow velocity data, the vorticity field presented in Fig. 2 was computed. The vortex is shown to have a bimodal vorticity distribution, which is probably due to the rollup process of the vorticity sheets from the oscillating airfoil. When integrated, the vorticity field yields a circulation of 0.49 m^2/s.

Flow Visualization Methods

Flow visualization of the interaction process was obtained using a laser sheet lighting system. Vaporized kerosene, ejected from the center of the trailing edge of the vortex generator, was illuminated by the laser sheet using the encoder signal as a time reference. The laser beam was split into two beams fanned out on either side of the blade model (to minimize shadows) by two cylindrical lenses. Laser light strobe times on the order of 10 μs were used to freeze the flow optically while the image was recorded on videotape. The system was capable of firing one shot per cycle, and the illuminated portion of the cycle was advanced during the run such that a slow-motion video of the interaction cycle was produced containing about 250 frames of data per cycle.

In order to extract quantitative data from the videotape, a video output from a graphics terminal was superimposed on the flow visualization video signal using a video special-effects generator. Using an interactive graphics program, registration lines inscribed on the front side plate window were "traced" and recorded onto a data file. Then, on a frame-by-frame basis, vortices were traced with ellipses, which were moved to the correct position, expanded, elongated, and rotated to

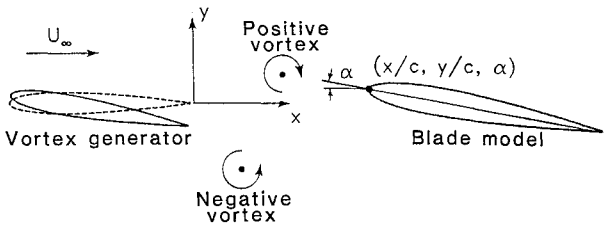

Fig. 1 Coordinate system definition.

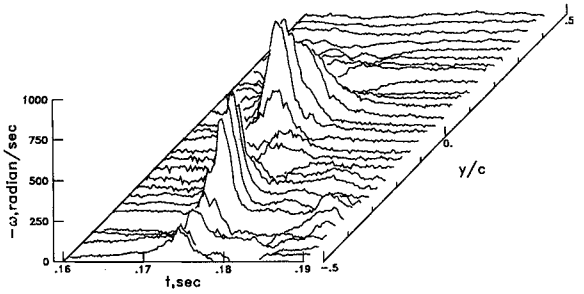

Fig. 2 Vorticity field produced by tailored wake.

match the vortex feature most closely. Parameters for the ellipse were then recorded on the data file. Ellipse position, size, and distortion data were scaled using registration line data. Position data were used to determine vortex velocity by computing the distance traveled between two frames and dividing by twice the time difference between frames, resulting in a space-centered approximation to the velocity. This method of velocity calculation resulted in a rather crude estimate of the vortex velocity because the time interval between frames was so small that the distance traveled by the vortex was of the same order as the position measurement error. As a result, some discretion is advised in interpretation of vortex convection velocity data, although general trends observed in the data are examined.

Unsteady Surface Pressure Measurements

Finally, unsteady pressures on the surface of the blade model were measured by connecting standard 1.27-cm microphones to long tubes connected to pressure ports on the blade surface, along the centerline of the blade model. Because of the length and narrow size of the pressure tubing, a sine sweep calibration was performed to determine amplitude and phase characteristics of the system. These calibration data were used in the data processing, and the maximum frequency retained in the data was 500 Hz, limiting the resolution of the unsteady loading and acoustic field calculations based on these data. Further tests should incorporate transducers with much higher-frequency responses. As discussed in the next section, the unsteady blade surface pressure was used to compute not only transient blade loading but the acoustic field produced by the interaction.

First, the unsteady blade surface pressure was integrated over the surface of the airfoil leading edge to compute the transient loading undergone by the blade. This integration was performed over the leading 25% of the blade chord, but the rms value of the unsteady pressure was shown to diminish[17] by the 0.20 c station, so that the remainder of the blade surface is not expected to contribute to the total transient lift. The transient forces were resolved into lift and were nondimensionalized using the measured mean velocity at the leading-edge station to form the transient lift coefficient data presented.

Of course, the main motivation behind this study is the noise generation process associated with two-dimensional BVI. However, the test rig was too noisy to measure the acoustic field directly. On the other hand, calculation of the acoustic field from the unsteady blade surface pressure data is feasible. In fact, several studies have been conducted using measured blade surface pressure data to predict acoustic results, which are then compared to experimental measurements of the acoustic field. One such study[20] resulted in excellent agreement between measured and predicted acoustic pressure waveforms. Encouraged by these favorable results, the present study used the unsteady blade surface pressure data to calculate the acoustic field around the blade using Farassat's formulation 1A.[19] In his formulation 1A, Farassat breaks the sound pressure integrals into two portions: those integrals that contribute to acoustic pressure because of blade loading and those that contribute on account of blade thickness. (Note: Here $f = 0$ refers to the blade surface and not to zero frequency.)

$$p'(\boldsymbol{x},t) = p'_L(\boldsymbol{x},t) + p'_T(\boldsymbol{x},t) \tag{1}$$

$$\begin{aligned} 4\pi p'_L(\boldsymbol{x},t) = {} & \frac{1}{c_0}\int_{f=0}\left[\frac{\dot{l}_i\hat{r}_i}{r(1-M_r)^2}\right]_{\text{ret}} \mathrm{d}S \\ & + \int_{f=0}\left[\frac{l_r - l_iM_i}{r^2(1-M_r)^2}\right]_{\text{ret}} \mathrm{d}S \\ & + \frac{1}{c_0}\int_{f=0}\left[\frac{l_r(r\dot{M}_i\hat{r}_i + c_0M_r - c_0M^2)}{r^2(1-M_r)^3}\right]_{\text{ret}} \mathrm{d}S \end{aligned} \tag{2}$$

$$4\pi p'_T(\boldsymbol{x},t) = \int_{f=0}\left[\frac{\rho_0 v_n(r\dot{M}_i\hat{r}_i + c_0M_r - c_0M^2)}{r^2(1-M_r)^3}\right]_{\text{ret}} \mathrm{d}S \tag{3}$$

For this analysis, the integrals in Eq. (2) were retained, as the unsteady blade surface pressure data represent unsteady loading. Since the blade is stationary in a low-speed flow, no significant effect due to blade thickness is expected, and so the integrals in Eq. (3) were neglected.

Two further simplifications were used in this analysis. First, the force on the fluid l, equal to the product $P_{ij}n_i$, was composed of two parts corresponding to steady and unsteady portions of the pressure matrix. It can be shown that the steady pressure distribution of the airfoil contributes a steady acoustic pressure, which would not be measured by a microphone system. Therefore, the unsteady surface pressure, which is what was measured on the blade surface, is used to compute the acoustic field. The other simplification was the assumption that the steady freestream velocity was the only velocity acting on the blade. Because of the low Mach number of the freestream velocity, and even lower Mach number for the perturbation velocities, this assumption is reasonable.

The integrals in Eq. (2) were evaluated over the surface of the leading 25% of the blade chord by dividing the blade surface into panels 1 c wide, centered about the pressure ports. The acoustic field was evaluated at radii of 1 and 100 c in front of the blade, using the blade leading edge as the center of the arc to compare the near- and far-field acoustic waveforms.

Results

This section will describe the effects of the encounter process on the vortex trajectory, size, and shape. Then, the effects of the interaction on blade unsteady loading will be examined. Finally, computations of the acoustic field expected to be radiated from these two-dimensional BVI will be discussed.

Interaction Process Effects on the Vortex

Flow visualization reveals a number of changes occurring in the vortex as the vortex intercepts the blade model, including changes in vortex trajectory, size, and shape. The cases chosen here represent the direct and nearly direct encounter cases, where viscous effects such as vortex core distortion are most apparent. The vortex generator is fixed to the side plate so

that, in order to vary blade-to-vortex miss distance, the position of the blade model was changed. The four blade positions chosen for this presentation are with the leading edge positioned at $y/c = -0.063$, -0.094, -0.125, and -0.219. All four cases are repeated for 0 and 10-deg angles of attack. It should be noted that in the absence of the blade model, the undisturbed vortex crosses the plane of the blade leading edge at $y/c = -0.063$.

One way to detect trends in trajectory data is to normalize vortex trajectory data by the blade leading-edge position (i.e., plot x/c, y/c distances relative to the blade leading edge). Trajectory plots normalized to leading-edge position are presented in Fig. 3. Note that, in Fig. 3a for the $\alpha = 0$ deg condition, in three cases, the vortex travels below the blade model. For the $y/c = -0.063$ case, the vortex is merely redirected below the blade. The $y/c = -0.94$ case shows that the vortex is turned a bit more than in the last case, but it also passes beneath the blade. In the $y/c = -0.125$ case, the vortex split into two fragments, which traveled on both the upper and lower surfaces of the blade. The remnant on the upper surface of the blade could not be tracked long since it diffused rapidly. In the last case, $y/c = -0.219$, the vortex burst as it approached the leading edge, and the remnants of the vortex were too diffuse to track. It is interesting that the vortices are able to pass below the blade with relatively little effect but that a vortex attempting to pass over the blade was disrupted rapidly.

When the blade angle of attack is set to 10 deg, as plotted in Fig. 3b, for the $y/c = -0.219$ case, the vortex is deflected over the blade. Unlike the $\alpha = 0$ deg case, the vortex is not appreciably disrupted as it passes over the blade. The next two cases involve a direct blade-vortex encounter, where the vortex collides with the blade leading edge. For the $y/c = -0.125$ case, the vortex splits at the leading edge, and portions of the vortex travel on both sides of the blade. This time, the vortex remnant on the lower surface dissipates relatively quickly while the remnant on the upper surface, although distorted, survives the encounter. When the blade is moved to $y/c = -0.094$, the vortex again collides with the blade leading edge, but this time the vortex remnant on the lower surface is the survivor. Apparently, the split of vorticity between the vortex remnants is determined by the precise blade-to-vortex geometry and, if the split is unequal, the remnant obtaining most of the vorticity survives longer as a coherent structure. Perhaps, somewhere between the cases of $y/c = -0.125$ and -0.094, there exists a point at which the vorticity split is equal and both vortex remnants may survive. For $y/c = -0.063$, the vortex is once again deflected below the blade.

Vortex streamwise convection velocity obtained from flow visualization data is presented in Fig. 4. The vortex convection velocity data are normalized by the measured mean velocity of 4.6 m/s. An interesting observation from the data presented in Fig. 4 is that the vortices seem to move unsteadily through the test section. In Fig. 4a, for the $\alpha = 0$ deg cases, velocity minima are seen to be grouped around $t = 0.008$ s and $t = 0.018$ s. A third group of minima occur around $t = 0.027$ s. In Fig. 4b, velocity minima (for all but the $y/c = -0.219$ case, which displays a velocity maximum) occur around $t = 0.009$, 0.021, and 0.030 s. The minima in the vortex streamwise velocity may be related to unsteady blade loading and, therefore, noise production.

Another set of data obtained from the flow visualization concerns the degree to which the normally circular vortex core becomes elongated. For this study, the vortex core was matched to an ellipse to reveal vortex distortion through ellipse parameters a/c, the length of the ellipse major axis, and the eccentricity e. For a circular undistorted vortex, a/c equals the core radius normalized by the blade chord length, and e equals zero. For both the $\alpha = 0$ and 10 deg cases, the vortex core radius a/c tends toward a general linear expansion (from $a/c = 0.025$ to 0.050) as the test section is traversed. The only major exception to this observation is $y/c = -0.125$, where the vortex expands in the vicinity of the blade leading edge. Recall, from earlier discussion, that this case represents a direct encounter, so that this perturbation is actually due to elongation of the core as a result of the collision.

Thus, it seems that, in general, the vortices expand as they traverse the test section and become much more elliptical.

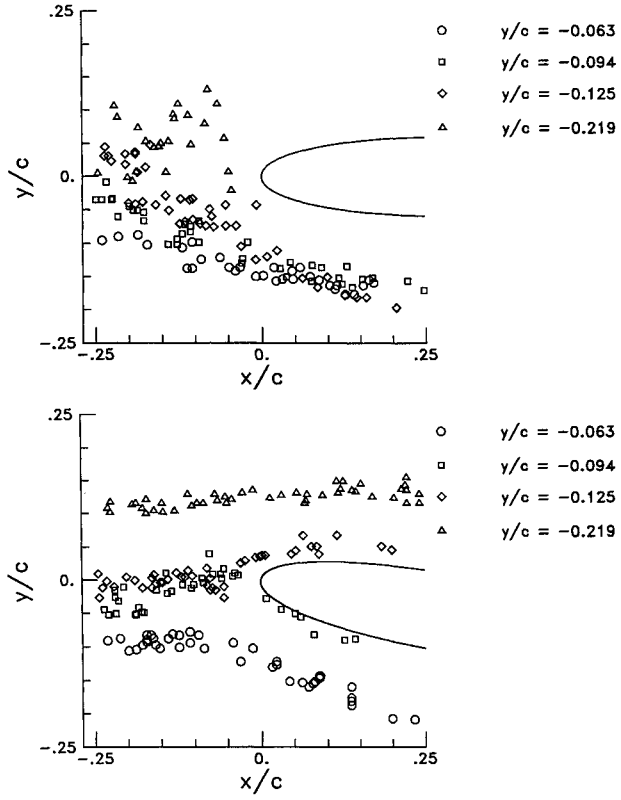

Fig. 3 Vortex trajectory data: a) $\alpha = 0$ deg cases; b) $\alpha = 10$ deg cases.

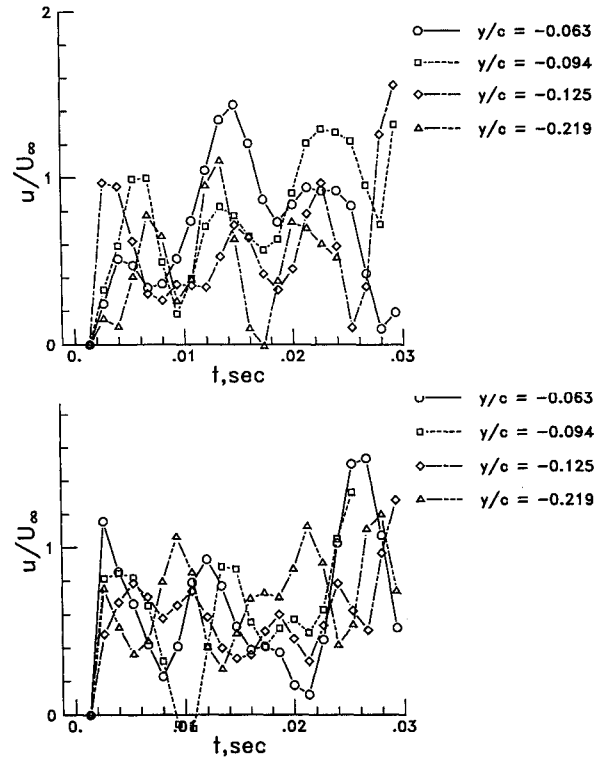

Fig. 4 Vortex convection velocity time history: a) $\alpha = 0$ deg cases; b) $\alpha = 10$ deg cases.

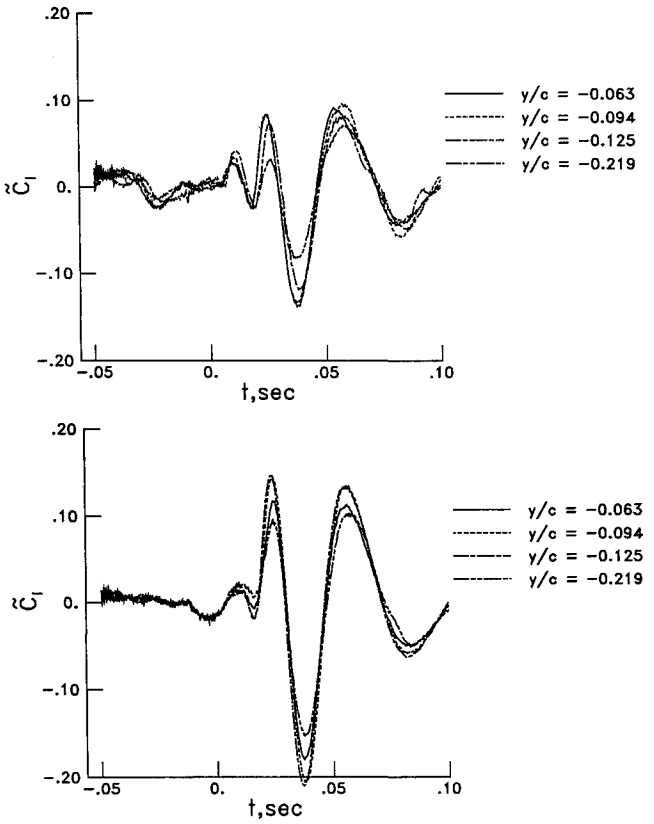

Fig. 5 Blade transient loading time history: a) $\alpha = 0$ deg cases; b) $\alpha = 10$ deg cases.

Although there is no clear trend to relate vortex distortion to blade angle of attack, the trajectories of the vortices are affected, with the $\alpha = 10$ deg case bending the vortex trajectories in the direction of the circulation of the blade. Finally, although several cases of direct encounter are examined here and vortex splitting occurs, it seems that only the vortex remnant that inherited most of the vorticity from the original vortex survives for any great length of time, the other remnant dispersing rapidly.

Interaction Process Effects on Blade Transient Loading

Up to this point, we have examined the effects of the interaction process on the vortex; we now turn to the effects of the interaction process on the blade. In Fig. 5a, the transient loading time histories on the blade for $\alpha = 0$ deg are presented. Although all four cases are similar in waveform, the amplitude of the $y/c = -0.219$ case is noticeably less than the other three. Recall that this is the case in which the vortex structure burst as it attempted to pass over the blade model. Evidently, the premature dissolution of the organized vortex structure is related to the decrease in amplitude of transient loading. Other subtle differences in the data show that the $y/c = -0.063$ case exhibits peak loads slightly before the two intermediate cases. Also, the shape of the second loading maximum is more rounded for the $y/c = -0.094$ and -0.125 cases. This is possibly due to the higher degree of elongation of the vortices for these cases, resulting in a wider vortex feature, which may take longer to traverse the blade.

Figure 5b shows the corresponding data for $\alpha = 10$ deg. First, compared with the previous plot, the amplitudes of the transient loading are increased with blade angle of attack. Next, it is almost immediately recognizable that maximum loading occurs with the two cases identified as direct encounter cases. In fact, although the vortex remnant for $y/c = -0.094$ passed beneath the blade whereas the $y/c = -0.125$ case passed over the upper surface, there is no appreciable difference in the transient loading time history. It is conjectured that the case in which an equal split of vorticity occurs, i.e., somewhere between the two cases examined, would yield the maximum amplitude of transient loading. Finally, the fact that the $y/c = -0.063$ case (in which the vortex passed beneath the blade) causes a larger-amplitude transient loading than the $y/c = -0.125$ case (in which the vortex passes over the blade) may be due to the fact that the vortex passing beneath the blade is closer to the blade than the vortex passing over the blade. Once again, the sharpness of the second loading maximum may be due to the degree of vortex elongation, which is less for the $y/c = -0.219$ case than for the $y/c = -0.063$ case.

Thus, the near-field vortex behavior is seen to influence transient loading time history. The importance of the blade-to-vortex miss distance is seen to influence the amplitude of loading, whereas vortex velocity may influence the timing of loading pulses. The degree to which the vortex core becomes noncircular may have an influence over the sharpness of the loading pulses, particularly for the second maximum in the loading cycle. Finally, the blade angle of attack has a major influence on the amplitude of the transient blade loading.

Interaction Process Effects on the Radiated Acoustic Field

In this section, the acoustic pressure waveforms computed from the unsteady blade surface pressure data are presented for observer radii of 1 and 100 c. The near-field acoustic waveforms for $\alpha = 0$ deg are presented in Fig. 6a. It is evident that the two cases with strongest near-field radiation are $y/c = -0.063$ and -0.094. It is interesting that the $y/c = -0.219$ case, in which the vortex burst, exhibits the weakest signal. In the far-field data, Fig. 6b, it is interesting to note that the acoustic amplitude of the acoustic waveform depends on the blade-to-vortex spacing, whereas the width of the waveform is independent of this parameter. It is also apparent that a burst vortex does not produce as intense a pulse as a less disrupted vortex.

In Fig. 6c, the near-field acoustic waveforms for the blade $\alpha = 10$ deg case are presented. As before, the most intense pulses are evident for $y/c = -0.094$ and -0.125, cases exhibiting significant vortex distortion. As with the loading data, the least intense case here is $y/c = -0.219$, with $y/c = -0.063$ producing an intermediate signal. In Fig. 6d, the timing of pressure extrema are once again practically independent of blade-to-vortex spacing. The direct encounter cases produce the largest acoustic pressure amplitudes, whereas less direct encounter geometries produce smaller amplitudes.

An interesting feature of the acoustic data is the pattern of a positive pressure peak surrounded by the pressure minima; qualitatively, this acoustic pulse shape is similar to data acquired below the rotor disk from the advancing side of model rotor undergoing BVI noise conditions.[20-22] Qualitative similarity in the acoustic waveform is not in itself sufficient to allow us to say conclusively that the two-dimensional BVI and the BVI measured in model tests result from the same process. Although scaling of the amplitude of the acoustic pulse is difficult as a result of various scaling factors as well as frequency limitations in the present data, it is not terribly difficult to check scaling of the pulse width. Pulse width time for the data in Fig. 6 is about 0.042 s. At a velocity of 4.6 m/s, a vortex would travel 0.945 c in that interval, or about one chord length. This effectively defines the interaction interval to be the length of time required for the rotor blade to pass through, or by, the vortex. It is expected that the minimum interaction interval would occur during two-dimensional BVI and that a nonparallel BVI interaction interval should be longer, depending on blade-to-vortex interaction angle and vortex geometry.

A first-order estimation[7] of blade section velocity during the interaction, assuming that the interaction occurs at 3/4 blade radius on the advancing side of the rotor disk, is given by

$$U = U_\infty + 3/4 V_{tip} \tag{4}$$

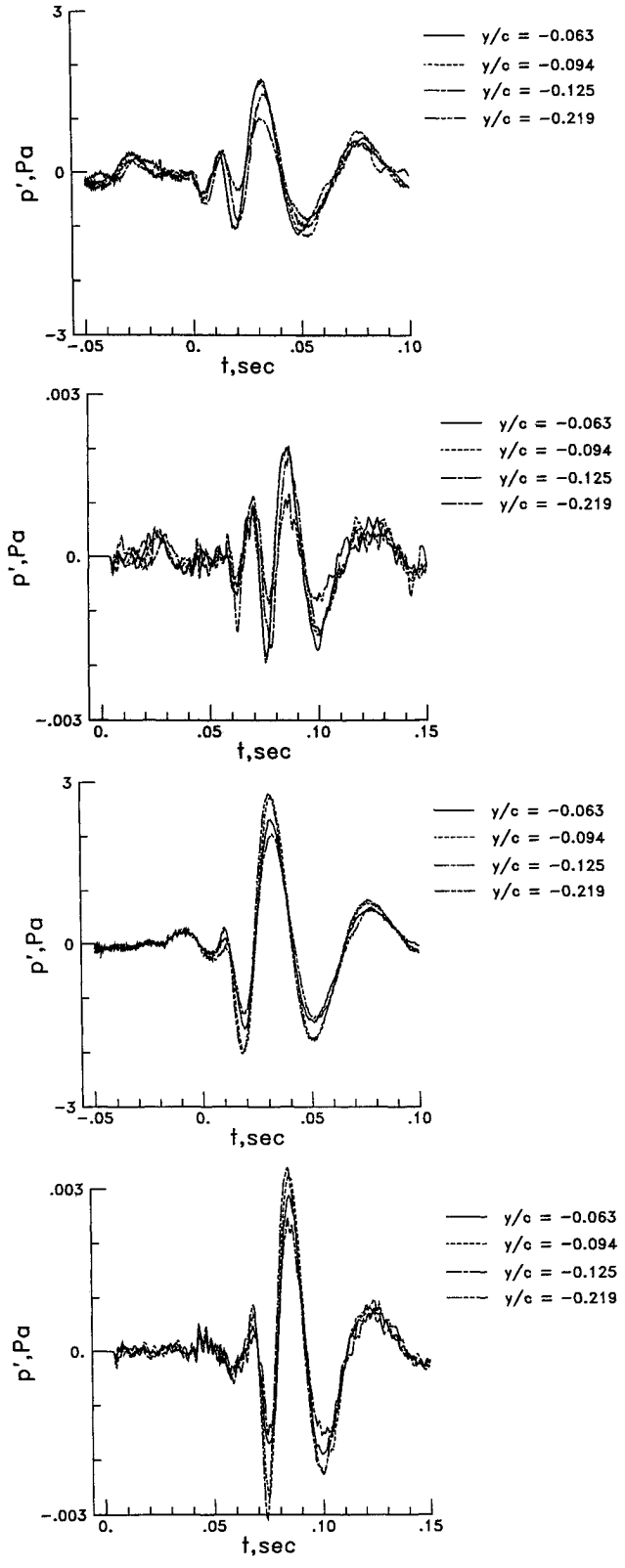

Fig. 6 Acoustic pressure time history: a) $\alpha = 0$ deg, $r/c = 1$; b) $\alpha = 0$ deg, $r/c = 100$; c) $\alpha = 10$ deg, $r/c = 1$; d) $\alpha = 10$ deg, $r/c = 100$.

where U_∞ is the wind-tunnel freestream velocity and V_{tip} is the rotational velocity of the blade tip. From Refs. 20–22, acoustic pulse widths were measured and U was calculated. The resulting interaction length is normalized by blade chord length. As noted before, the resulting interaction length from two-dimensional BVI is about 1. Data from Ref. 20, a test of a four-bladed rotor, result in interaction lengths near 1, suggesting that a nearly two-dimensional BVI encounter took place. References 21 and 22 concern two-bladed rotors and produce interaction lengths from 2 to 5, suggesting nonparallel type of BVI encounters. Although inconclusive until flow visualization of BVI in model rotors reveal true BVI geometry, it is interesting that the experimental data did not show a pulse width narrower than the two-dimensional case. For the degree of analysis possible here, it is concluded that the similarity in acoustic pressure waveform between the two-dimensional BVI data and model rotor acoustic data is reasonably good.

Conclusions

Two-dimensional blade-vortex interaction has been studied experimentally by immersing an airfoil model representing a rotor blade section into the wake generated by another airfoil model oscillating in a nonsinusoidal tailored oscillation pattern. The resulting wake contains isolated vortices separated by about five chord lengths that have a circulation of 0.49 m^2/s, with a mean velocity of 4.6 m/s, where the leading edge of the blade model was positioned.

Flow visualization data reveal that blade loading has no discernible effect on vortex core expansion. Blade loading was seen to affect vortex trajectory, convection velocity, and core distortion strongly. One case demonstrated bursting of the vortex, whereas vortex splitting was observed for three of the eight cases presented. In those cases in which vortex splitting was evident, the portion of the vortex that inherited most of the vorticity survived as a coherent flow feature longer than the weaker vortex remnant.

Transient loading data, calculated from unsteady blade surface pressures, show trends consistent with observations made from flow visualization data, primarily that the amplitude of blade transient loading was increased by blade angle of attack and reduction of the blade-to-vortex distance.

Calculations of the acoustic waveforms generated by the interaction process were presented. Amplitudes for the direct encounter cases were higher than for the near-miss cases, and amplitudes for the blade $\alpha = 10$ deg were higher than for the $\alpha = 0$ deg cases. The current study suggests that reduction in blade steady loading or an increase in the blade-vortex miss distance will reduce blade transient loading as well as noise produced by the blade-vortex interaction.

References

[1]Widnall, S., "Helicopter Noise Due to Blade-Vortex Interaction," *Journal of the Acoustical Society of America,* Vol. 50, July 1971, pp. 354–365.

[2]Nakamura, Y., "Prediction of Blade Vortex Interaction from Measured Blade Pressure," AHS Seventh European Rotorcraft Powered Lift Forum, 1981.

[3]Hardin, J. C., and Lamkin, S. L., "Aeroacoustic Interaction of a Distributed Vortex with a Lifting Joukowski Airfoil," AIAA Paper 84-2287, Oct. 1984.

[4]Wu, J. C., Sankar, N. L., and Hsu, T. M., "Unsteady Aerodynamics of an Airfoil Encountering a Passing Vortex," AIAA Paper 85-0203, Jan. 1985.

[5]George, A. R., and Chang, S. B., "Noise Due to Transonic Blade-Vortex Interactions," AHS 39th Annual Forum, May 1983.

[6]McCroskey, W. J., and Goorjian, P. M., "Interactions of Airfoils with Gusts and Concentrated Vortices in Transonic Flow," AIAA Paper 83-1691, July 1983.

[7]Hardin, J. C., and Lamkin, S. L., "Concepts for Reduction of Blade/Vortex Interaction Noise," *Journal of Aircraft,* Vol. 24, Feb. 1987, pp. 120–125.

[8]Bratt, J. B., "Flow Patterns in the Wake of an Oscillating Aerofoil," A.R.C., R&M 2773, 1953.

[9]Poling, D. R., and Telionis, D. P., "Response of Airfoils to Periodic Disturbances—The Unsteady Kutta Condition, *AIAA Journal,* Vol. 24, Feb. 1986, pp. 193–199.

[10]Robinson, M. C., and Luttges, M. W., "Control of Wake Structure Behind an Oscillating Airfoil," AIAA Paper 86-2282-CP, Aug. 1986.

[11]Booth, E. R., and Yu, J. C., "Two-Dimensional Blade-Vortex Flow Visualization Investigation," *AIAA Journal,* Vol. 24, Sept. 1986, pp. 1468–1473.

[12]Katz, J., and Weihs, D., "Behavior of Vortex Wakes from Oscillating Airfoils," *Journal of Aircraft,* Vol. 15, 1978, pp. 861–863.

[13]Theodorsen, T., "General Theory of Aerodynamic Instability and the Mechanism of Flutter," NACA TR-496, 1935.

[14]Sears, W. R., "Some Aspects of Non-Stationary Airfoil Theory and Its Practical Application," *Journal of Aeronautical Science,* Vol. 8, Jan. 1941, pp. 104–108.

[15]Booth, E. R. and Yu, J. C., "New Technique for Experimental Generation of Two Dimensional Blade-Vortex Interaction at Low Reynolds Numbers," NASA TP-2551, March 1986.

[16]Booth, E. R., "Measurement of Velocity and Vorticity Fields in the Wake of an Airfoil in Pitching Motion," NASA TP-2780, Dec. 1987.

[17]Booth, E. R., "Surface Pressure Measurement During Low Speed Blade-Vortex Interaction," AIAA Paper 86-1856, July 1986.

[18]Hubbard, H. H., and Manning, J. C., "Aeroacoustic Research Facilities at NASA Langley Research Center—Description and Operational Characteristics," NASA TM-84585, 1983.

[19]Farassat, F., and Succi, G. P., "The Prediction of Helicopter Rotor Discrete Frequency Noise," *Vertica,* Vol. 7, 1983, pp. 309–320.

[20]Shultz, K., and Splettstoesser, W. R., "Prediction of Helicopter Rotor Impulsive Noise Using Measured Blade Pressures," presented at the 43rd Annual Forum and Technology Display of the American Helicopter Society, St. Louis, MO, May 1987.

[21]Schmitz, F. H., Boxwell, D. A., Lewy, S., and Dahan, C., "Model to Full-Scale Comparisons of Blade-Vortex Interaction Noise," *Journal of the American Helicopter Society,* Vol. 29, April 1984.

[22]Hoad, D. R., "Helicopter Blade-Vortex Interaction Locations-Scale-Model Acoustics and Free-Wake Analysis Results," NASA TP-2658, April 1987.